Research Article

Large Deflection Analysis of Graphene Sheets in the Thermal Environment Using Higher-Order Nonlocal Strain Gradient Principle

Mostafa Sadeghian *, Mahmoud Shariati [ID]

Department of Mechanical Engineering, Faculty of Engineering, Ferdowsi University of Mashhad, Mashhad, Iran

ARTICLE INFO

ABSTRACT

This paper investigates the large deflection of a sector nanoplate on the Winkler elastic foundation in the thermal environment based on the nonlocal strain gradient principle. By taking into account von Karman's nonlinear strains and applying the higher-order shear deformation theory (HSDT), the governing equations of the graphene plate are derived. By presenting acceptable accuracy without the need for a shear correction coefficient, HSDT eliminates the defects of the first shear deformation theory (FSDT) and provides an appropriate distribution for shear stress along the thickness. The equations have been solved using the differential quadrature method (DQM) and the extended Kantorovich method (EKM). The results of the present study are compared with the available references, which demonstrate good agreement among them. For example, the results of the present study for the radius ratios of 0.25, 0.5, and 0.75 have 0.35%, 2.83%, and 7% differences with Ref. [1]. In conclusion, this study examines the impact of various small-scale parameters, load, boundary conditions, geometric dimensions, and elastic foundation on the maximum nondimensional deflection in the thermal environment.

1. Introduction

In recent decades, nanotechnology has revolutionized science and consumer products. It has the potential to create a wide domain of novel products, including materials used in the generation of energy, biomaterials, and electronics. Usually, it involves developing materials or electronics that can be integrated into structures that are at least one dimension smaller than 100 nm [2]. Nanostructures include graphene sheets, nano rings, carbon nanotubes, nanowires, and nanorods, which are created by forming graphene sheets [3]. For this reason, the analysis of graphene sheets is the main topic when examining carbon nanomaterials. The graphene sheet is as thick as a carbon atom and is placed in a hexagonal crystal lattice that has unique mechanical characteristics, including high flexibility, high tensile strength, high thermal and electrical conductivity, etc.

Experimental observations have demonstrated that the mechanical properties of structures at the nanoscale can be different from those at the macroscale. For this reason, classical continuum mechanics models cannot predict the characteristics of nanostructures because of their inability to examine small-scale effects. To overcome these obstacles, non-classical continuum mechanics models have been

* Corresponding author.
  E-mail address: msadeghian@um.ac.ir

developed, including the nonlocal elasticity principle, couple stress principle, strain gradient principle, etc. These models provide a more thorough understanding of the mechanical properties of nanoscale structures and were created to address the shortcomings of classical approaches. To be more specific, Eringen [4] introduced a nonlocal elasticity model that adds nonlocal effects to classical elasticity theory. According to this principle, the stress at a point is affected by the entire material domain.

There are different investigations in the case of analyzing structures based on different theories such as FSDT [4-6], HSDT [7], etc. Trabelsi et al. [5] examined the thermal post-buckling of FGM shells based on the nonlinear modified FSDT. In another paper, Trabelsi et al. [6] investigated the thermal buckling of FGM plates and shells using modified FSDT. Also, Zghal et al. [7] analyzed the nonlinear large deflection of FG carbon nanotube-reinforced panels and plates based on FSDT via a finite element technique. For example, Joueid et al. [8] studied the thermoelastic buckling of FG porous plates and shells with an efficient finite element model using modified FSDT. In another study, Zghal et al. [9] examined the time-deflection responses of FG porous spherical shells and plates exposed to various external pulse excitations. By extending the Kirchhoff-Love model, Trabelsi et al. [10] studied thermal buckling and post-buckling analysis of FG plates and shells. Zghal et al. [11] perused vibration investigation of FG composite shells made of carbon nanotubes. Zghal et al. [12] investigated the vibration of FGM beams based on a mixed formulation. Zghal and her colleagues [13] investigated the post-buckling of plates and panels made of FGM and carbon nanotube-reinforced composites exposed to various mechanical loads.

Recently, many investigations related to nanostructure analyses have been published. Zghal et al. [14] examined static investigation of FG carbon nanotube-reinforced structures. In another paper, they [15] carried out research about the buckling of functionally graded carbon nanotube-reinforced composite structures. The authors of Ref. [16] analyzed the dynamic investigation of FG carbon nanotube-reinforced structures. The nonlinear bending of FG carbon nanotube-reinforced structures was studied by Zghal and her colleagues [17]. Mehar et al. [18] investigated the vibration of a nanoplate using a novel higher-order model via the finite-element method and nonlocal elasticity theory.

For considering strain gradient effects, Mindlin [19] and Aifantis [20] introduced the strain gradient component to the classical elasticity principle. Lam and his coauthors [21] introduced the modified strain gradient principle that considers the influence of strain gradients, including dilatation gradient, symmetry rotation gradient, and deviatoric stretch gradient. In these theories, the strain gradient influence or the nonlocal role is taken into account. To assume these effects for computations of nanostructures, the nonlocal strain gradient principle was applied by Lim et al. [22]. Based on the nonlocal strain gradient principle, numerous studies have been carried out on the size-dependent mechanical behavior of nanostructures. For instance, using the nonlocal strain gradient model, Gui and Wu [23] conducted research about the buckling of the thermo-magneto-electro-elastic nanocylindrical shell exposed to axial load. They observed that the effect of the nonlocal coefficient on the buckling load of nano cylindrical shells is more significant than that of the strain gradient parameter. Lu and his colleagues [24] proposed a size-dependent classical model to investigate the buckling analysis of rectangular nanoplates. Using the nonlocal strain gradient principle and FSDT, the bending of the sandwich nanoplates with porosity was presented by Arefi et al. [25]. In addition, Farajpour and his colleagues [26] perused the buckling of orthotropic nanoplates exposed to thermal conditions based on the higher-order nonlocal strain gradient principle. They observed that the higher-order nonlocal parameter almost has a decreasing influence on the buckling load. Moreover, the authors of Ref. [27] applied the same theory to study the nonlinear vibration of sandwich nanoplates. They concluded that by enhancing the amplitude of vibrations, the influence of small-scale parameters on the nonlinear frequency becomes more significant. Thai et al. [28] studied free vibrations of functionally graded circular/annular nanoplates made of magneto-electro-elastic materials via the nonlocal strain gradient principle. They showed that the non-dimensional natural frequencies obtained from circular nanoplates are higher than those predicted for annular types.

The large deflection analysis of the plate is one of the important topics in the engineering field, which attracts many researchers [29-31]. For instance, Liu et al. [32] studied the large deflection of a thin rectangular plate exposed to uniform loads. Wang and Xiao [33] investigated the bending examination of the rectangular nanolaminates using the Kirchhoff theory and the Gurtin-Murdoch surface elasticity model. They concluded that surface effects decrease the deflections. Mehar et al. [34] conducted research on the bending analysis of nanotube-reinforced sandwich structures exposed to Mehar and Panda [18] perused the bending of multi-walled carbon nanotube-reinforced sandwich panels

theoretically and experimentally. In another paper, Mehar and his colleagues [35] studied the static and vibrational examination of the FG carbon nanotube-reinforced sandwich plate in the thermal environment via the finite element method. Also, Mehar et al. [36] examined the nonlinear bending of FG carbon nanotube-reinforced panels in the thermal environment based on higher-order theory. Moreover, the authors of Ref. [37] analyzed the bending of carbon nanotube-reinforced plate Experimentally, theoretically, and numerically. Mehar et al. [38] studied the nonlinear bending of nanotube-reinforced panels numerically and experimentally.

In this article, the nonlocal strain gradient theory and HSDT for examining the large deflection of the sector nanoplate in the thermal environment are presented. Also, the roles of geometry, the elastic foundation, loads, sector angle, radius, small-scale parameters, and different boundary conditions are studied.

2. The Governing Equations

Figure 1. illustrates the graphene sector plate on the Winkler elastic foundation with r_i and r_o as the internal and outer radii, respectively. Moreover, the sector angle and the thickness of the plate are defined by τ and h.
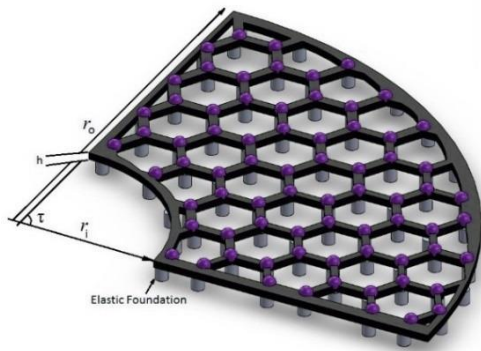

Fig. 1. The schematic of the graphene sector plate on the Winkler elastic foundation

Using the HSDT, the displacement field can be obtained in the r, θ, and z directions (signified by U, V, and W, respectively) as:

$$U(r,\theta,z) = u_0(r,\theta) - z\frac{\partial w_0(r)}{\partial r} + g(z)\phi(r,\theta)$$
$$V(r,\theta,z) = v_0(r,\theta) - \frac{z}{r}\frac{\partial w_0(r,\theta)}{\partial \theta} + g(z)\psi(r,\theta) \qquad (1)$$
$$W(r,\theta,z) = w_0(r,\theta)$$

where u_0, v_0, and w_0 can be assumed as the displacement components of the midplane along the r, θ, and z axes. Besides, ψ and ϕ are the rotation components in the r and θ directions. Moreover, the function $g(z)$ can be clarified as:

$$g(z) = f(z) + zy^* \qquad (2)$$

$f(z)$ and y^* can be assumed as several functions that have been utilized in different references summarized in Table 1.

Table 1. Some g(z) functions are used in various papers

Model	$g(z)$ function
Ambartsumian [39]	$-\frac{1}{6}z^3 + \frac{h^2}{8}z$
Reddy [40]	$-\frac{4}{3h^2}z^3 + z$
Reissner [41]	$-\frac{5}{3h^2}z^3 + \frac{5}{4}z$
Touratier [42]	$\frac{h}{\pi}\sin\left(\frac{\pi z}{h}\right)$
Soldatos [43]	$h\sinh\left(\frac{z}{h}\right) - z\cosh\left(\frac{1}{2}\right)$
Aydogdu [44]	$ze^{-2\left(\frac{z}{h}\right)^2}$
Mantari [45]	$\frac{h}{\pi}\left(\sin\left(\frac{\pi z}{h}\right)e^{m\cos\left(\frac{\pi z}{h}\right)} + m\frac{\pi}{h}z\right)$

Using the presumptions of von Karman, the nonlinear strain components considering thermal effects are as follows:

$$\varepsilon_r = \frac{\partial u_0}{\partial r} - z\frac{\partial^2 w_0}{\partial r^2} + g(z)\frac{\partial \phi}{\partial r} + \frac{1}{2}\left(\frac{\partial w_0}{\partial r}\right)^2 - \alpha_{11}\Delta T \qquad (3)$$

$$\varepsilon_\theta = \frac{1}{r}\left(u_0 - z\frac{\partial w_0}{\partial r} + \frac{\partial v_0}{\partial \theta} - \frac{z}{r}\frac{\partial^2 w_0}{\partial \theta^2} + g(z)\left(\frac{\partial \psi}{\partial \theta} + \phi\right)\right)$$
$$+ \frac{1}{2}\left(\frac{1}{r}\frac{\partial w_0}{\partial \theta}\right)^2 - \alpha_{22}\Delta T \qquad (4)$$

$$\gamma_{r\theta} = \frac{1}{r}\left(\frac{\partial u_0}{\partial \theta} - 2z\frac{\partial^2 w_0}{\partial r\partial \theta} + g(z)\frac{\partial \phi}{\partial \theta} + \frac{\partial w_0}{\partial \theta}\frac{\partial w_0}{\partial r} - v_0 - g(z)\psi\right)$$
$$+ 2\frac{z}{r^2}\frac{\partial w_0}{\partial \theta} + \frac{\partial v_0}{\partial r} + g(z)\frac{\partial \psi}{\partial r} \qquad (5)$$

$$\gamma_{rz} = \phi\frac{\partial g(z)}{\partial z} \qquad (6)$$

$$\gamma_{\theta z} = \psi\frac{\partial g(z)}{\partial z} \qquad (7)$$

The stress and moment resultants with the nonlocal form (*NL*) are as follows:

$$\{N_r, N_\theta, N_{r\theta}, Q_r, Q_\theta\}^{NL} = \int_{-\frac{h}{2}}^{\frac{h}{2}} \{\sigma_r, \sigma_\theta, \sigma_{r\theta}, \sigma_{rz}, \sigma_{\theta z}\}^{NL} dz \quad (8)$$

$$\{M_r, M_\theta, M_{r\theta}\}^{NL} = \int_{-\frac{h}{2}}^{\frac{h}{2}} \{\sigma_r, \sigma_\theta, \sigma_{r\theta}\}^{NL} z dz \quad (9)$$

$$\{R_r, R_\theta, R_{r\theta}\}^{NL} = \int_{-\frac{h}{2}}^{\frac{h}{2}} \{\sigma_r, \sigma_\theta, \sigma_{r\theta}\}^{NL} f(z) dz \quad (10)$$

$$\{R_{rz}, R_{\theta z}\}^{NL} = \int_{-\frac{h}{2}}^{\frac{h}{2}} \{\sigma_{rz}, \sigma_{\theta z}\}^{NL} f'(z) dz \quad (11)$$

The potential energy of the system includes the sum of the strain energy (related to the internal forces work) and the potential energy (related to external forces):

$$\Pi = U + \Omega \quad (12)$$

Π can be assumed as the potential energy of the whole system, *U* defines the strain energy of the system and Ω is the potential energy of external forces. Using the minimum potential energy principle when the system is in equilibrium condition, the variation of the potential energy is equal to zero:

$$\delta\Pi = \delta U + \delta\Omega = 0 \quad (13)$$

The integral over the volume of the strain energy density should be considered in order to write the variations of the system's strain energy. The following is the strain energy density:

$$\delta u_v = \sigma_{ij}\delta\varepsilon_{ij} \quad (14)$$

Moreover, for strain energy variations, the following equation is considered:

$$\delta U = \iiint_V \delta u_v dV = \iiint_V \sigma_{ij}\delta\varepsilon_{ij} dV \quad (15)$$

Therefore:

$$\delta U = \iiint_V (\sigma_r\delta\varepsilon_r + \sigma_\theta\delta\varepsilon_\theta + \sigma_{r\theta}\delta\gamma_{r\theta} + \sigma_{rz}\delta\gamma_{rz} + \sigma_{z\theta}\delta\gamma_{z\theta}) dV \quad (16)$$

Also:

$$\delta\Omega = -\iint_A (q - k_w w_0) r \delta w_0 dr d\theta \quad (17)$$

where k_w defines the Winkler elastic foundation constant. Therefore:

$$\delta\Pi = \delta\Omega + \delta U$$
$$= -\int_0^{2\pi}\int_0^r (q - k_w w_0) r \delta w_0 dr d\theta + \delta U = 0 \quad (18)$$

Considering $\delta\Pi$ equal to zero, the coefficients of $\delta u_0, \delta w_0$ and $\delta\phi$ should be zero, and the Euler-Lagrange equations are computed in the non-local form (with superscript NL) as follows:

$$\delta u_0 : N_r^{NL} - N_\theta^{NL} + r\frac{\partial N_r^{NL}}{\partial r} + \frac{\partial N_{r\theta}^{NL}}{\partial\theta} = 0 \quad (19)$$

$$\delta v_0 : \frac{\partial N_\theta^{NL}}{\partial\theta} + r\frac{\partial N_{r\theta}^{NL}}{\partial r} + 2N_{r\theta}^{NL} = 0 \quad (20)$$

$$\delta w_0 : r\frac{\partial^2 M_r^{NL}}{\partial r^2} + 2\frac{\partial M_r^{NL}}{\partial r} - \frac{\partial M_\theta^{NL}}{\partial r} + \frac{1}{r}\frac{\partial^2 M_\theta^{NL}}{\partial\theta^2} + \frac{2}{r}\frac{\partial M_{r\theta}^{NL}}{\partial\theta} + 2\frac{\partial^2 M_{r\theta}^{NL}}{\partial\theta\partial r} + (q - k_w w_0)r + N_r^{NL}\frac{\partial w_0}{\partial r} + rN_r^{NL}\frac{\partial^2 w_0}{\partial r^2} + \frac{\partial N_r^{NL}}{\partial r}\frac{\partial w_0}{\partial r} r - r\frac{\partial w_0}{\partial r} + \frac{1}{r}N_\theta\frac{\partial^2 w_0}{\partial\theta^2} + \frac{1}{r}\frac{\partial N_\theta^{NL}}{\partial\theta}\frac{\partial w_0}{\partial\theta} + \frac{\partial N_{r\theta}^{NL}}{\partial\theta}\frac{\partial w_0}{\partial r} + \frac{\partial N_{r\theta}^{NL}}{\partial r}\frac{\partial w_0}{\partial\theta} + 2N_{r\theta}^{NL}\frac{\partial^2 w_0}{\partial r\partial\theta} = 0 \quad (21)$$

$$\delta\psi : y^*\left(r\frac{\partial M_{r\theta}^{NL}}{\partial r} + \frac{\partial M_\theta^{NL}}{\partial\theta} + 2M_{r\theta}^{NL} - rQ_\theta^{NL}\right) + 2R_{r\theta}^{NL} - rR_{z\theta}^{NL} + r\frac{\partial R_{r\theta}^{NL}}{\partial r} + \frac{\partial R_\theta^{NL}}{\partial\theta} = 0 \quad (22)$$

$$\delta\phi : y^*\left(r\frac{\partial M_r^{NL}}{\partial r} + \frac{\partial M_{r\theta}^{NL}}{\partial\theta} + M_r^{NL} - M_\theta^{NL} - rQ_r^{NL}\right) + R_r^{NL} - R_\theta^{NL} + r\frac{\partial R_r^{NL}}{\partial r} + \frac{\partial R_{r\theta}^{NL}}{\partial\theta} - rR_{rz}^{NL} = 0 \quad (23)$$

Also, Eq. 21 can be written as:

$$\delta w_0 : r\frac{\partial^2 M_r^{NL}}{\partial r^2} + 2\frac{\partial M_r^{NL}}{\partial r} - \frac{\partial M_\theta^{NL}}{\partial r} + \frac{1}{r}\frac{\partial^2 M_\theta^{NL}}{\partial\theta^2} + \frac{2}{r}\frac{\partial M_{r\theta}^{NL}}{\partial\theta} + 2\frac{\partial^2 M_{r\theta}^{NL}}{\partial\theta\partial r} + (q - k_w w_0)r + rN_r^{NL}\frac{\partial^2 w_0}{\partial r^2} + N_\theta^{NL}\frac{\partial w_0}{\partial r} + \frac{1}{r}N_\theta^{NL}\frac{\partial^2 w_0}{\partial\theta^2} - \frac{2}{r}N_{r\theta}^{NL}\frac{\partial w_0}{\partial\theta} + 2N_{r\theta}^{NL}\frac{\partial^2 w_0}{\partial r\partial\theta} = 0 \quad (24)$$

The nonlocal strain gradient principle was developed by Lim et al.[22] and is explained as follows (which can be considered as the combination of the strain gradient model and nonlocal stresses field):

$$(1 - \mu^2\nabla^2)\sigma_{ij} = C_{ijkl}(1 - l^2\nabla^2)\varepsilon_{kl},$$
$$\nabla^2 = \frac{\partial^2}{\partial r^2} + \frac{1}{r^2}\frac{\partial^2}{\partial\theta^2} + \frac{1}{r}\frac{\partial}{\partial r} \quad (25)$$

In the above equation, the coefficients denoting nonlocal, elastic, and strain gradients (or internal material length scales) are μ, C_{ijkl} and l, respectively. Moreover, the constitutive equation for stress-strain at the nanoscale is shown as [46]:

$$\begin{bmatrix} \sigma_r \\ \sigma_\theta \\ \sigma_{r\theta} \\ \sigma_{rz} \\ \sigma_{\theta z} \end{bmatrix} = \begin{bmatrix} Q_{11} & Q_{12} & 0 & 0 & 0 \\ Q_{12} & Q_{22} & 0 & 0 & 0 \\ 0 & 0 & G_{12} & 0 & 0 \\ 0 & 0 & 0 & G_{13} & 0 \\ 0 & 0 & 0 & 0 & G_{23} \end{bmatrix} \begin{bmatrix} \varepsilon_r \\ \varepsilon_\theta \\ \gamma_{r\theta} \\ \gamma_{rz} \\ \gamma_{\theta z} \end{bmatrix} \tag{26}$$

$$\begin{cases} Q_{11} = \dfrac{E_1}{1-v_{12}v_{21}} \quad, \quad Q_{22} = \dfrac{E_2}{1-v_{12}v_{21}} \\ Q_{12} = \dfrac{v_{12}E_2}{1-v_{12}v_{21}} \end{cases}$$

In the above equation, E_1 and E_2 are the Young's modulus along 1 and 2 directions. Also, v_{12} and v_{21} are Poisson's ratios. Moreover, G_{12}, G_{13} and G_{23} are the shear moduli.

The nonlocal form can be written as follows:

$$(1-\mu\nabla^2)\{N_r, N_\theta, N_{r\theta}, Q_r, Q_\theta\}^{NL} =$$
$$\int_{-\frac{h}{2}}^{\frac{h}{2}} (1-\mu\nabla^2)\{\sigma_r, \sigma_\theta, \sigma_{r\theta}, \sigma_{rz}, \sigma_{\theta z}\}^{NL} dz \tag{27}$$

In the local form, the force and moment resultants are as follows:

$$\{N_r, N_\theta, N_{r\theta}, Q_r, Q_\theta\}^L = \int_{-\frac{h}{2}}^{\frac{h}{2}} \{\sigma_r, \sigma_\theta, \sigma_{r\theta}, \sigma_{rz}, \sigma_{\theta z}\}^L dz \tag{28}$$

$$\{M_r, M_\theta, M_{r\theta}\}^L = \int_{-\frac{h}{2}}^{\frac{h}{2}} \{\sigma_r, \sigma_\theta, \sigma_{r\theta}\}^L z\,dz \tag{29}$$

$$\{R_r, R_\theta, R_{r\theta}\}^L = \int_{-\frac{h}{2}}^{\frac{h}{2}} \{\sigma_r, \sigma_\theta, \sigma_{r\theta}\}^L f(z)\,dz \tag{30}$$

$$\{R_{rz}, R_{\theta z}\}^L = \int_{-\frac{h}{2}}^{\frac{h}{2}} \{\sigma_{rz}, \sigma_{\theta z}\}^L f'(z)\,dz \tag{31}$$

Also, the following forms of resultants are gained in terms of displacements:

$$N_r^L = (1-l^2\nabla^2)\frac{1}{1-v_{12}v_{21}}\left(E_1 h\left(\frac{\partial u_0}{\partial r} + \frac{1}{2}\left(\frac{\partial w_0}{\partial r}\right)^2\right) + v_{12}E_2 h\left(\frac{1}{r}u_0 + \frac{1}{r}\frac{\partial v_0}{\partial \theta} + \frac{1}{2}\left(\frac{1}{r}\frac{\partial w_0}{\partial \theta}\right)^2\right) + \left(E_1\frac{\partial \phi}{\partial r} + v_{12}E_2\frac{1}{r}\left(\frac{\partial \psi}{\partial \theta}+\phi\right)\right)\int_{-\frac{h}{2}}^{\frac{h}{2}}f(z)dz\right)$$
$$- \frac{h\Delta T(E_2\alpha_{22}v_{12} + E_1\alpha_{11})}{1-v_{12}v_{21}} \tag{32}$$

$$N_\theta^L = (1-l^2\nabla^2)\frac{E_2}{1-v_{12}v_{21}}\left(v_{12}h\left(\frac{\partial u_0}{\partial r} + \frac{1}{2}\left(\frac{\partial w_0}{\partial r}\right)^2\right) + h\left(\frac{1}{r}\left(u_0 + \frac{\partial v_0}{\partial \theta}\right) + \frac{1}{2}\left(\frac{1}{r}\frac{\partial w_0}{\partial \theta}\right)^2\right) + \left(v_{12}\frac{\partial \phi}{\partial r} + \left(\frac{\partial \psi}{\partial \theta}+\phi\right)\right)\int_{-\frac{h}{2}}^{\frac{h}{2}}f(z)dz\right)$$
$$- \frac{E_2 h\Delta T(\alpha_{11}v_{12} + E_1\alpha_{22})}{1-v_{12}v_{21}} \tag{33}$$

$$N_{r\theta}^L = (1-l^2\nabla^2)G_{12}\left(h\left(\frac{1}{r}\frac{\partial u_0}{\partial \theta} + \frac{1}{r}\frac{\partial w_0}{\partial \theta}\frac{\partial w_0}{\partial r} - \frac{1}{r}v_0 + \frac{\partial v_0}{\partial r}\right) + \left(\frac{1}{r}\frac{\partial \phi}{\partial \theta} - \frac{1}{r}\psi + \frac{\partial \psi}{\partial r}\right)\int_{-\frac{h}{2}}^{\frac{h}{2}}f(z)dz\right) \tag{34}$$

$$M_r^L = (1-l^2\nabla^2)\frac{1}{1-v_{12}v_{21}}\left(\begin{array}{l} E_1\frac{h^3}{12}\left(-\frac{\partial^2 w_0}{\partial r^2} + y^*\frac{\partial \phi}{\partial r}\right) \\ + v_{12}E_2\frac{h^3}{12}\left(-\frac{1}{r}\frac{\partial w_0}{\partial r} - \frac{1}{r^2}\frac{\partial^2 w_0}{\partial \theta^2} + y^*\frac{1}{r}\left(\frac{\partial \psi}{\partial \theta}+\phi\right)\right)\end{array}\right) + \left(E_1\frac{\partial \phi}{\partial r} + v_{12}E_2\frac{1}{r}\left(\frac{\partial \psi}{\partial \theta}+\phi\right)\right)\int_{-\frac{h}{2}}^{\frac{h}{2}}zf(z)dz\right) \tag{35}$$

$$M_\theta^L = (1-l^2\nabla^2)\frac{E_2}{1-v_{12}v_{21}}\left(v_{12}\frac{h^3}{12}\left(-\frac{\partial^2 w_0}{\partial r^2} + y^*\frac{\partial \phi}{\partial r}\right) + \frac{h^3}{12}\left(-\frac{1}{r}\frac{\partial w_0}{\partial r} - \frac{1}{r^2}\frac{\partial^2 w_0}{\partial \theta^2} + y^*\frac{1}{r}\left(\frac{\partial \psi}{\partial \theta}+\phi\right)\right) + \left(v_{12}\frac{\partial \phi}{\partial r} + \frac{1}{r}\left(\frac{\partial \psi}{\partial \theta}+\phi\right)\right)\int_{-\frac{h}{2}}^{\frac{h}{2}}zf(z)dz\right) \tag{36}$$

$$M_{r\theta}^L = (1-l^2\nabla^2)G_{12}\frac{h^3}{12}\left(-\frac{2}{r}\frac{\partial^2 w_0}{\partial r\partial \theta} + \frac{2}{r^2}\frac{\partial w_0}{\partial \theta} + y^*\left(\frac{1}{r}\frac{\partial \phi}{\partial \theta} - \frac{1}{r}\psi + \frac{\partial \psi}{\partial r}\right) + \left(\frac{1}{r}\frac{\partial \phi}{\partial \theta} - \frac{1}{r}\psi + \frac{\partial \psi}{\partial r}\right)\int_{-\frac{h}{2}}^{\frac{h}{2}}zf(z)dz\right) \tag{37}$$

$$R_r^L = (1-l^2\nabla^2)\frac{1}{1-v_{12}v_{21}}\left\{\left(E_1\left(\frac{\partial u_0}{\partial r} + \frac{1}{2}\left(\frac{\partial w_0}{\partial r}\right)^2\right) + v_{12}E_2\left(\frac{1}{r}u_0 + \frac{1}{r}\frac{\partial v_0}{\partial \theta} + \frac{1}{2}\left(\frac{1}{r}\frac{\partial w_0}{\partial \theta}\right)^2\right)\right)\int_{-\frac{h}{2}}^{\frac{h}{2}}f(z)dz\right.$$
$$\left. + \left(E_1\left(-\frac{\partial^2 w_0}{\partial r^2} + y^*\frac{\partial \phi}{\partial r}\right) + v_{12}E_2\left(-\frac{1}{r}\frac{\partial w_0}{\partial r} - \frac{1}{r^2}\frac{\partial^2 w_0}{\partial \theta^2} + y^*\frac{1}{r}\left(\frac{\partial \psi}{\partial \theta}+\phi\right)\right)\right)\int_{-\frac{h}{2}}^{\frac{h}{2}}zf(z)dz + \left(E_1\frac{\partial \phi}{\partial r} + v_{12}E_2\frac{1}{r}\left(\frac{\partial \psi}{\partial \theta}+\phi\right)\right)\int_{-\frac{h}{2}}^{\frac{h}{2}}(f(z))^2 dz\right\} \tag{38}$$

$$R_\theta^L = (1-l^2\nabla^2)\frac{E_2}{1-v_{12}v_{21}}\left\{\left(v_{12}\left(\frac{\partial u_0}{\partial r} + \frac{1}{2}\left(\frac{\partial w_0}{\partial r}\right)^2\right) + \left(\frac{1}{r}u_0 + \frac{1}{r}\frac{\partial v_0}{\partial \theta} + \frac{1}{2}\left(\frac{1}{r}\frac{\partial w_0}{\partial \theta}\right)^2\right)\right)\int_{-\frac{h}{2}}^{\frac{h}{2}}f(z)dz + \right.$$
$$\left. \left(v_{12}\left(-\frac{\partial^2 w_0}{\partial r^2} + y^*\frac{\partial \phi}{\partial r}\right) + \left(-\frac{1}{r}\frac{\partial w_0}{\partial r} - \frac{1}{r^2}\frac{\partial^2 w_0}{\partial \theta^2} + y^*\frac{1}{r}\left(\frac{\partial \psi}{\partial \theta}+\phi\right)\right)\right)\int_{-\frac{h}{2}}^{\frac{h}{2}}zf(z)dz + \left(v_{12}\frac{\partial \phi}{\partial r} + \frac{1}{r}\left(\frac{\partial \psi}{\partial \theta}+\phi\right)\right)\int_{-\frac{h}{2}}^{\frac{h}{2}}(f(z))^2 dz\right\} \tag{39}$$

$$R_{r\theta}^L = (1-l^2\nabla^2)\left\{G_{12}\left(\frac{1}{r}\frac{\partial u_0}{\partial \theta} + \frac{1}{r}\frac{\partial w_0}{\partial \theta}\frac{\partial w_0}{\partial r} - \frac{1}{r}v_0 + \frac{\partial v_0}{\partial r}\right)\int_{-\frac{h}{2}}^{\frac{h}{2}}f(z)dz + G_{12}\left(-\frac{2}{r}\frac{\partial^2 w_0}{\partial r\partial \theta} + \frac{2}{r^2}\frac{\partial w_0}{\partial \theta} + y^*\left(\frac{1}{r}\frac{\partial \phi}{\partial \theta} - \frac{1}{r}\psi + \frac{\partial \psi}{\partial r}\right)\right)\int_{-\frac{h}{2}}^{\frac{h}{2}}zf(z)dz\right.$$
$$\left. + G_{12}\left(\frac{1}{r}\frac{\partial \phi}{\partial \theta} - \frac{1}{r}\psi + \frac{\partial \psi}{\partial r}\right)\int_{-\frac{h}{2}}^{\frac{h}{2}}(f(z))^2 dz\right\} \tag{40}$$

$$Q_r^L = (1 - l^2 \nabla^2) G_{13} \left(\phi \int_{-\frac{h}{2}}^{\frac{h}{2}} f'(z) dz + h y^* \phi \right) \tag{41}$$

$$Q_\theta^L = (1 - l^2 \nabla^2) G_{23} \left(\psi \int_{-\frac{h}{2}}^{\frac{h}{2}} f'(z) dz + h y^* \psi \right) \tag{42}$$

$$R_{rz}^L = (1 - l^2 \nabla^2)$$
$$\{ (G_{13} \phi \int_{-\frac{h}{2}}^{\frac{h}{2}} (f'(z))^2 dz + G_{13} y^* \phi \int_{-\frac{h}{2}}^{\frac{h}{2}} f'(z) dz) \} \tag{43}$$

$$R_{\theta z}^L = (1 - l^2 \nabla^2) \{ G_{23} \psi \int_{-\frac{h}{2}}^{\frac{h}{2}} (f'(z))^2 dz$$
$$+ G_{23} y^* \psi \int_{-\frac{h}{2}}^{\frac{h}{2}} f'(z) dz \} \tag{44}$$

The following equations represent the local expression of the equilibrium equations for sector nanoplate on the elastic foundation:

$$\delta u_0 : N_r^L - N_\theta^L + r \frac{\partial N_r^L}{\partial r} + \frac{\partial N_{r\theta}^L}{\partial \theta} = 0 \tag{45}$$

$$\delta v_0 : \frac{\partial N_\theta^L}{\partial \theta} + r \frac{\partial N_{r\theta}^L}{\partial r} + 2 N_{r\theta}^L = 0 \tag{46}$$

$$\delta w_0 : r \frac{\partial^2 M_r^L}{\partial r^2} + 2 \frac{\partial M_r^L}{\partial r} - \frac{\partial M_\theta^L}{\partial r} + \frac{1}{r} \frac{\partial^2 M_\theta^L}{\partial \theta^2} + \frac{2}{r} \frac{\partial M_{r\theta}^L}{\partial \theta} +$$
$$2 \frac{\partial^2 M_{r\theta}^L}{\partial \theta \partial r} + (1 - \mu \nabla^2) \left((q - k_w w_0) r + r N_r^L \frac{\partial^2 w_0}{\partial r^2} + \right.$$
$$N_\theta^L \frac{\partial w_0}{\partial r} + \frac{1}{r} N_\theta^L \frac{\partial^2 w_0}{\partial \theta^2} - \frac{2}{r} N_{r\theta}^L \frac{\partial w_0}{\partial \theta} + 2 N_{r\theta}^L \frac{\partial^2 w_0}{\partial r \partial \theta} \right) +$$
$$\mu r \left((\nabla^2 N_r^L) \frac{\partial^2 w_0}{\partial r^2} + (\nabla^2 N_\theta^L) \left(\frac{1}{r} \frac{\partial w_0}{\partial r} + \frac{1}{r^2} \frac{\partial^2 w_0}{\partial \theta^2} \right) \right.$$
$$\left. + 2 (\nabla^2 N_{r\theta}^L) \left(\frac{1}{r} \frac{\partial^2 w_0}{\partial r \partial \theta} - \frac{1}{r^2} \frac{\partial w_0}{\partial \theta} \right) \right) = 0 \tag{47}$$

$$\delta \phi : y^* \left(r \frac{\partial M_r^L}{\partial r} + \frac{\partial M_{r\theta}^L}{\partial \theta} + M_r^L - M_\theta^L - r Q_r^L \right) +$$
$$R_r^L - R_\theta^L + r \frac{\partial R_r^L}{\partial r} + \frac{\partial R_{r\theta}^L}{\partial \theta} - r R_{rz}^L = 0 \tag{48}$$

$$\delta \psi : y^* \left(r \frac{\partial M_{r\theta}^L}{\partial r} + \frac{\partial M_\theta^L}{\partial \theta} + 2 M_{r\theta}^L - r Q_\theta^L \right) +$$
$$2 R_{r\theta}^L - r R_{z\theta}^L + r \frac{\partial R_{r\theta}^L}{\partial r} + \frac{\partial R_\theta^L}{\partial \theta} = 0 \tag{49}$$

Also, the boundary conditions can be considered as the following relations:

- Simply supported (S):

$$u = v = w = \psi = M_r = R_r = 0 \qquad r = r_i, \ r_o$$
$$u = v = w = \varphi = M_\theta = R_\theta = 0 \qquad \theta = 0, \ \tau \tag{50}$$

- Clamped (C):

$$u = v = w = \psi = M_r = R_r = 0 \qquad r = r_i, \ r_o$$
$$u = v = w = \varphi = M_\theta = R_\theta = 0 \qquad \theta = 0, \ \tau \tag{51}$$

- Free (F):

$$u = v = w = \psi = M_r = R_r = 0 \qquad r = r_i, \ r_o$$
$$u = v = w = \varphi = M_\theta = R_\theta = 0 \qquad \theta = 0, \ \tau \tag{52}$$

3. The Solution Method

The extended Kantorovich method (EKM) [47] is used to convert the two-dimensional equations into one-dimensional forms, and then they are solved by the one-dimensional differential quadratic method. Using the EKM, the bivariate function becomes the product of two univariate functions, as follows:

$$f(r, \theta) = f_1(r) \times g_1(\theta) \tag{53}$$

Also, displacement and rotation functions can be written as:

$$u(r, \theta) = f_1(r) \times g_1(\theta) \tag{54}$$

$$v(r, \theta) = f_2(r) \times g_2(\theta) \tag{55}$$

$$w(r, \theta) = f_3(r) \times g_3(\theta) \tag{56}$$

$$\phi(r, \theta) = f_4(r) \times g_4(\theta) \tag{57}$$

$$\psi(r, \theta) = f_5(r) \times g_5(\theta) \tag{58}$$

Using the above relationships in the equilibrium relations, differential equations with partial derivatives become ordinary differential relations. With the arbitrary initial choice of the functions $g_i, i = 1..5$, the equilibrium relations will be obtained based on the weighted Galerkin residual method. In this method, the governing equations should be multiplied by a suitable function in terms of θ, and after integration in terms of θ, ordinary differential equations will be obtained, which will be only a function of $f_i, i = 1...5$. Consequently, by solving the ordinary differential relations and considering the boundary conditions, the f_i functions will be obtained:

$$\int_0^\tau g_1(\theta) \times e_1 d\theta = 0 \tag{59}$$

$$\int_0^\tau g_2(\theta) \times e_2 d\theta = 0 \tag{60}$$

$$\int_0^\tau g_3(\theta) \times e_3 d\theta = 0 \tag{61}$$

$$\int_0^\tau g_4(\theta) \times e_4 d\theta = 0 \tag{62}$$

$$\int_0^\tau g_5(\theta) \times e_5 d\theta = 0 \tag{63}$$

where, $e_1, e_2, ..., e_5$ are equilibrium equations.

Each of the equilibrium relations should be multiplied by the suitable function g_i and integrated with the range from 0 to τ with respect to θ. Therefore, the equilibrium equations (in the partial differential form) are converted into a system of ordinary differential equations in terms of *r*, which can be solved by taking into account the boundary conditions. By obtaining the f_i functions and placing them in the equilibrium relations, the ordinary differential relations are obtained in terms of *θ*, which g_i can be calculated by solving the differential equations.

Using the introduced functions, partial differential equations will be single-variable and become ordinary differential equations. Due to the non-linearity of the governing equations of the plate, numerical methods are used to solve the equations. One of the most efficient and accurate numerical solutions of differential equations is the differential quadrature method.

In two-dimensional analysis, there will be a set of nodes as shown in Figure 2. Using the Kantorovich method, calculations are reduced from two directions to one direction, which will cause a significant reduction in the number of calculations. For example, in the two-dimensional analysis, by selecting 9 nodes in each direction, the number of nodes is 81; if using the Kantorovich method, this number is reduced to only 9 points. Reducing the equations from 81 to 9 nonlinear equations will result in a huge reduction in calculations, which is one of the obvious advantages of using the Kantorovich method.
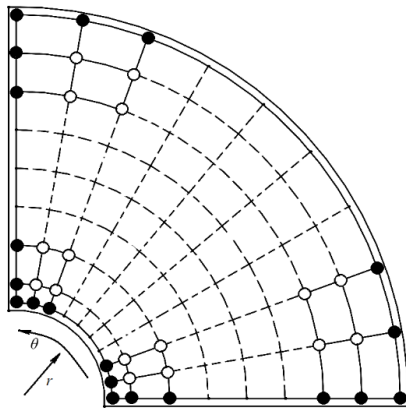

Fig. 2. Distribution of nodes in the geometry of the sector plate.

One of the most efficient and accurate numerical solutions to one-dimensional differential equations is the differential quadratic method. This method is one of the numerical methods with high precession obtained from the quadratic integration technique, where the integral at one node in the direction of the domain depends on all the nodes along that direction. It should be noted that weight coefficients determine the dependency's value: $f(r,\theta) = f_1(r) \times g_1(\theta)$ where weight coefficients and function values at discrete points can be clarified by $w_1, w_2, ..., w_n$ and $f_1, f_2, ..., f_n$, respectively.

Belman et al. [48] proposed that in quadratic integration, the derivative at a given point in the function domain is dependent upon the function values at every point in the domain through weight coefficients:

$$\left. \frac{df}{dr} \right|_{r_i} = \sum_{j=1}^N A_{ij} f(r_j) , \quad i = 1, 2, ..., N \tag{64}$$

A_{ij} can be defined as the weight parameter. Also, *N* refers to the total number of nodes in the direction of *r*. Moreover, the weighting coefficients for the first-order derivative are achieved as:

$$A_{ij}^{(1)} = \frac{P(r_i)}{(r_i - r_j) P(r_j)} \tag{65}$$

$$P(r_i) = \prod_{j=1}^N (r_i - r_j) , \quad i \neq j \tag{66}$$

$$A_{ii}^{(1)} = -\sum_{k=1}^N A_{ik}^{(1)} \quad , \quad i \neq k \tag{67}$$

Furthermore, regarding the higher-order derivatives:

$$\left. \frac{d^{(n)} f}{dr^{(n)}} \right|_{r_i} = \sum_{j=1}^N A_{ij}^{(n)} f(r_j) , \quad i = 1, ..., N \tag{68}$$

The following equations introduce the weighting coefficients for derivatives of the second and higher orders:

$$A_{ij}^{(n)} = n \left[A_{ij}^{(1)} A_{ii}^{(n-1)} - \frac{A_{ij}^{(n-1)}}{(r_i - r_j)} \right] , \quad i \neq j \tag{69}$$

$$\left. \frac{d^{(n)} f}{dr^{(n)}} \right|_{r_i} = \sum_{j=1}^N A_{ij}^{(n)} f(r_j) , \quad i = 1, ..., N \tag{70}$$

The grid point distribution used in this paper is on the basis of Chebyshev-Gauss-Lubato points,

which speeds up the solution's convergence and takes the following form:

$$r_i = \frac{r_i + r_o}{2} - \cos\left(\left(\frac{i-1}{N-1}\right)\pi\right)\left(\frac{r_o - r_i}{2}\right), i = 1...N \qquad (71)$$

In Eq. (70), the starting and ending points of the function are denoted by r_i and r_o, respectively.

4. Results and Discussions

This part investigates various factors based on HSDT and takes the nonlocal strain gradient model into consideration to determine how they affect the deflations of the sector nanoplate via EKM and DQM. To validate the current analysis and solution method, the results have been compared according to Table 2 for the CCCC boundary condition, taking into account the following presumptions:

$$E_1 = 1060(GPa) \quad , E_2 = 1060(GPa) \quad , v_{12} = 0.19 ,$$
$$v_{21} = 0.19 \quad , \quad \mu = 1(nm^2), k_w^* = 0.005331 \quad , k_p = 0 \quad , \quad (72)$$
$$h = 0.34(nm) \quad , r_i = 1(nm) \quad , r_o = 5(nm) \quad , \quad \theta = \pi.$$

which can be seen that the results of this paper are in good agreement with the reference. For example, the results of the present study for the radius ratios of 0.25, 0.5 and 0.75 have 0.5%, 1.1%, and 3.3% differences with references.

Table 2. The comparison of the dimensionless deflection gained by this paper with References for the sector sheet

r_i / r_o	*Non-dimensional deflection* $\overline{w} = (\frac{D}{qr_0^4})w \times 10^4$		
	Ref. [1]	*Ref. [49]*	*Present study*
0.25	*2.840*	*2.760*	*2.85*
0.5	*1.410*	*1.420*	*1.45*
0.75	*0.10*	*0.090*	*0.093*

The nondimensional deflection of the graphene sheet is compared with other references and gathered in Table 3. for SSSS boundary conditions and considering $\mu = 4(nm^2)$ which shows good harmony of the present results.

Table 3. The comparison of the dimensionless deflection gained by this paper with References for the graphene sheet

	The percentage of non-dimensional deflection	
q	Ref. [1]	Present study
0.1	0.56	0.58
0.5	2.8	2.69
1	5.6	5.88

By considering the following assumptions:

$$E_1 = 1765(GPa) \quad , E_2 = 1588(GPa) \quad ,$$
$$v_{12} = 0.3 \quad , v_{21} = 0.27, \quad q = 1(GPa) \quad ,$$
$$k_w^* = 0.005 \quad , h = 0.34(nm) \quad , r_o = 10(nm), \qquad (73)$$
$$\mu^* = 1, l^* = 0.025, \Delta T = 150K \quad ,$$
$$\alpha_{11} = 1.1*10^{-6}(K^{-1}) \quad , \alpha_{22} = \alpha_{11}/3.$$

The results of the present study are considered. It is noticed that various functions in Table 1. give similar results (so any of them can be chosen).

Figure 3 reveals the change of nondimensional maximum deflection versus nonlocal parameters for the sector nanoplate for diverse boundary conditions. It can be observed that by increasing the nonlocal parameter, the non-dimensional deflection decreases. This reduction is seen more noticeable when the boundary conditions are more flexible.
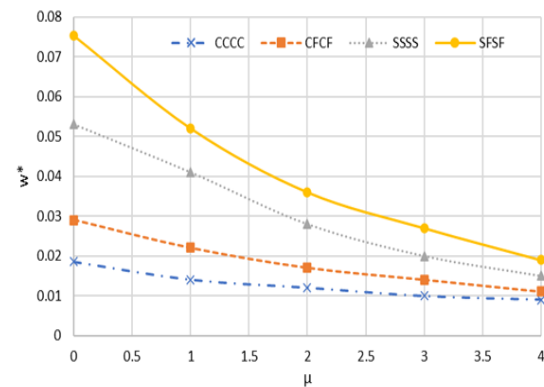

Fig. 3. The changes of dimensionless maximum deflection versus nonlocal parameter for the sector nanoplate

Figure 4 depicts the changes in dimensionless deflection versus bending loads. It is noted that by increasing the deflection, the deflection increases. Moreover, the difference in results between simply supporting boundary conditions and clamped conditions is more significant with the enhancement of the loads.
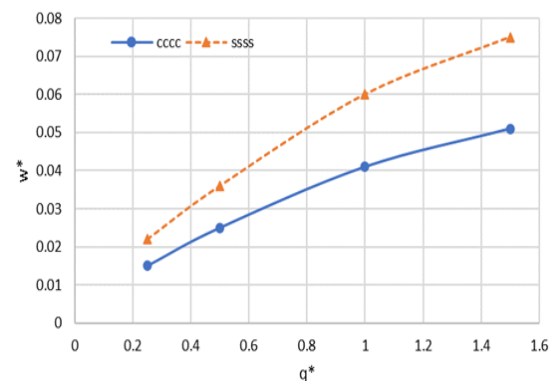

Fig 4. The variation of dimensionless maximum deflection versus bending loads for the sector graphene sheet

Figure 5 illustrates the changes in dimensionless deflection in terms of nondimensional radius for different boundary conditions. As can be seen, increasing the radius results in an enhancement of the deflection. Furthermore, increasing the radius causes a greater difference between the results of deflection in clamped and simply supported boundary conditions.
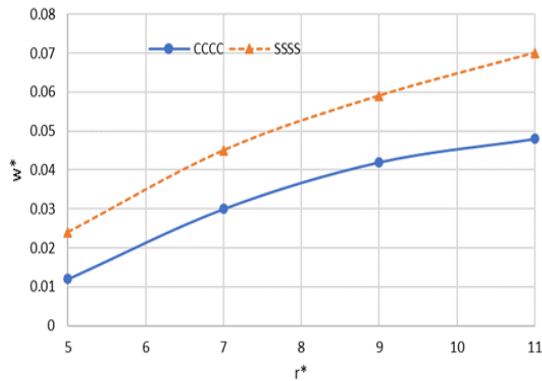

Fig. 5. The variation of dimensionless maximum deflection versus radius for the sector nanoplate

The changes in non-dimension deflection against the elastic foundation can be seen in Figure 6. It can be noticed that increasing the values of the elastic foundation causes a reduction in deflection values. Also, it can be noted that in the higher elastic foundation values, the deflection values for the clamped and simply supported boundary conditions are in close proximity to each other.
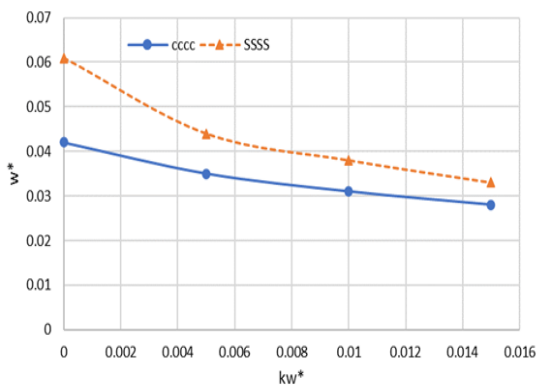

Fig. 6. The effect of the elastic foundation on the non-dimensional maximum deflection of the sector nanoplate

Figure 7 shows the influence of sector plate angle on non-dimensional deflection for different boundary conditions. It is noticed that by increasing the sector angle, the deflection increases. Also, it can be seen that the difference between boundary conditions is almost more significant at larger angles.
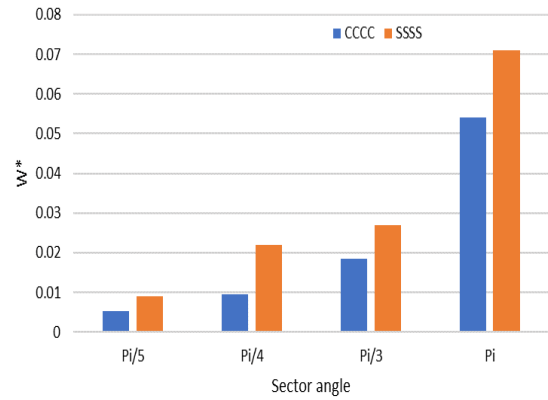

Fig. 7. The influence sector angle on the non-dimensional maximum deflection of the sector nanoplate

Figure 8 examines the difference between linear and nonlinear non-dimensional deflection for the clamped and simply supported boundary conditions.

It is clear that by increasing the nonlocal parameter, the difference increases for both boundary conditions, where the values of the simply supported condition show a more significant increase than the values of the clamped condition.
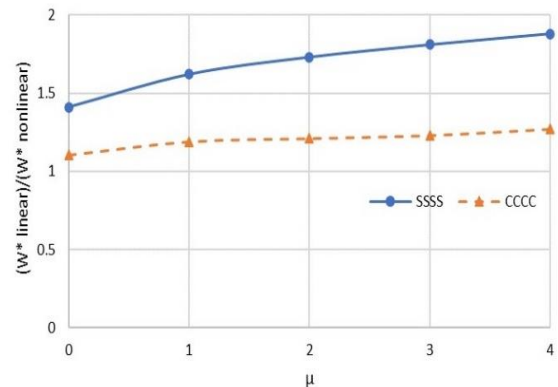

Fig. 8. The relation of nondimensional linear to nonlinear deflections versus nonlocal parameters.

Figure 9 illustrates the effect of the thermal environment on the non-dimensional deflection for the simply supported boundary condition.

In this figure, *Rt* is defined as follows:

$$Rt = \frac{\omega_{\text{with temperature}}}{\omega_{\text{without temperature}}} \tag{74}$$

It is clear that by increasing the temperature, the deflection increases.

Also, it can be seen that the difference between thermal conditions increases by enhancing the nonlocal parameter.
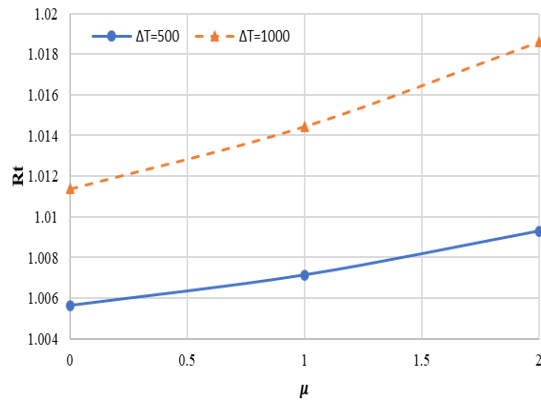
Fig. 9. The relation of nondimensional linear to nonlinear deflections versus nonlocal parameters

5. Conclusions

In this paper, the large deflection of the nanoplate in the thermal environment was studied with the aid of the nonlocal strain gradient theory with HSDT via DQM. The results were compared with a reference and showed good harmony. From the results of this paper, it can be noticed that:

∗ Factors such as radius, flexibility of boundary conditions, load, thermal condition, and sector angle have direct influences on the large deflection of the plate.

∗ Nonlocal parameters, elastic foundation, and rigidity of boundary conditions have countereffects on the large deflection of the plate.

Nomenclature

$U, V, W(r, \theta, z)$	Displacement functions
h	Thickness
τ	Sector angle
μ	Nonlocal parameter
l	Strain Gradient parameter
G	Shear module
v	Poisson's ratio
E	Young module

Funding Statement

Conflicts of Interest

The author(s) declared no potential conflicts of interest concerning the research, authorship, and publication of this article.

References

[1] Harik, I.E., 1984. Analytical solution to the orthotropic sector. *Journal of Engineering Mechanics, 110* (4)**,** pp.554-568.

[2] Kumar, R., Kumar, M. & Luthra, G., 2023. Fundamental approaches and applications of nanotechnology: A mini review. *Materials Today: Proceedings*.

[3] Farajpour, A., Mohammadi, M., Shahidi, A.R. & Mahzoon, M., 2011. Axisymmetric buckling of the circular graphene sheets with the nonlocal continuum plate model. *Physica E: Low-dimensional Systems and Nanostructures, 43* (10)**,** pp.1820-1825.

[4] Eringen, A.C., 1972. Nonlocal polar elastic continua. *International Journal of Engineering Science, 10* (1)**,** pp.1-16.

[5] Trabelsi, S., Frikha, A., Zghal, S. & Dammak, F., 2018. Thermal post-buckling analysis of functionally graded material structures using a modified fsdt. *International Journal of Mechanical Sciences, 144***,** pp.74-89.

[6] Trabelsi, S., Frikha, A., Zghal, S. & Dammak, F., 2019. A modified fsdt-based four nodes finite shell element for thermal buckling analysis of functionally graded plates and cylindrical shells. *Engineering Structures, 178***,** pp.444-459.

[7] Zghal, S., Frikha, A. & Dammak, F., 2020. Large deflection response-based geometrical nonlinearity of nanocomposite structures reinforced with carbon nanotubes. *Applied Mathematics and Mechanics, 41* (8), pp.1227-1250.

[8] Joueid, N., Zghal, S., Chrigui, M. & Dammak, F., 2023. Thermoelastic buckling analysis of plates and shells of temperature and porosity dependent functionally graded materials. *Mechanics of Time-Dependent Materials*.

[9] Zghal, S., Joueid, N., Tornabene, F., Dimitri, R., Chrigui, M. & Dammak, F., 2024. Time-dependent deflection responses of fg porous structures subjected to different external pulse loads. *Journal of Vibration Engineering & Technologies, 12* (1)**,** pp.857-876.

[10] Trabelsi, S., Zghal, S. & Dammak, F., 2020. Thermo-elastic buckling and post-buckling analysis of functionally graded thin plate and

shell structures. *Journal of the Brazilian Society of Mechanical Sciences and Engineering, 42* (5)**,** pp.233.

[11] Zghal, S., Frikha, A. & Dammak, F., 2018. Free vibration analysis of carbon nanotube-reinforced functionally graded composite shell structures. *Applied Mathematical Modelling, 53***,** pp.132-155.

[12] Zghal, S. & Dammak, F., 2020. Vibrational behavior of beams made of functionally graded materials by using a mixed formulation. *Proceedings of the Institution of Mechanical Engineers, Part C: Journal of Mechanical Engineering Science, 234* (18)**,** pp.3650-3666.

[13] Zghal, S., Trabelsi, S. & Dammak, F., 2022. Post-buckling behavior of functionally graded and carbon-nanotubes based structures with different mechanical loadings. *Mechanics Based Design of Structures and Machines, 50* (9)**,** pp.2997-3039.

[14] Zghal, S., Frikha, A. & Dammak, F., 2017. Static analysis of functionally graded carbon nanotube-reinforced plate and shell structures. *Composite Structures, 176***,** pp.1107-1123.

[15] Zghal, S., Frikha, A. & Dammak, F., 2018. Mechanical buckling analysis of functionally graded power-based and carbon nanotubes-reinforced composite plates and curved panels. *Composites Part B: Engineering, 150,* pp.165-183.

[16] Frikha, A., Zghal, S. & Dammak, F., 2018. Dynamic analysis of functionally graded carbon nanotubes-reinforced plate and shell structures using a double directors finite shell element. *Aerospace Science and Technology, 78***,** pp.438-451.

[17] Zghal, S., Frikha, A. & Dammak, F., 2018. Non-linear bending analysis of nanocomposites reinforced by graphene-nanotubes with finite shell element and membrane enhancement. *Engineering Structures, 158***,** pp.95-109.

[18] Mehar, K. & Panda, S.K., 2019. Theoretical deflection analysis of multi-walled carbon nanotube reinforced sandwich panel and experimental verification. *Composites Part B: Engineering, 167***,** pp.317-328.

[19] Mindlin, R.D., 1965. Second gradient of strain and surface-tension in linear elasticity. *International Journal of Solids and Structures, 1* (4)**,** pp.417-438.

[20] Aifantis, E.C., 1999. Strain gradient interpretation of size effects. *International Journal of Fracture, 95* (1)**,** pp.299-314.

[21] Lam, D.C.C., Yang, F., Chong, A.C.M., Wang, J. & Tong, P., 2003. Experiments and theory in strain gradient elasticity. *Journal of the Mechanics and Physics of Solids, 51* (8)**,** pp.1477-1508.

[22] Lim, C.W., Zhang, G. & Reddy, J.N., 2015. A higher-order nonlocal elasticity and strain gradient theory and its applications in wave propagation. *Journal of the Mechanics and Physics of Solids, 78***,** pp.298-313.

[23] Gui, Y. & Wu, R., 2023. Buckling analysis of embedded thermo-magneto-electro-elastic nano cylindrical shell subjected to axial load with nonlocal strain gradient theory. *Mechanics Research Communications, 128***,** pp.104043.

[24] Lu, L., Guo, X. & Zhao, J., 2019. A unified size-dependent plate model based on nonlocal strain gradient theory including surface effects. *Applied Mathematical Modelling, 68***,** pp.583-602.

[25] Arefi, M., Kiani, M. & Rabczuk, T., 2019. Application of nonlocal strain gradient theory to size dependent bending analysis of a sandwich porous nanoplate integrated with piezomagnetic face-sheets. *Composites Part B: Engineering, 168***,** pp.320-333.

[26] Farajpour, A., Yazdi, M.R.H., Rastgoo, A. & Mohammadi, M., 2016. A higher-order nonlocal strain gradient plate model for buckling of orthotropic nanoplates in thermal environment. *Acta Mechanica, 227* (7)**,** pp.1849-1867.

[27] Nematollahi, M.S. & Mohammadi, H., 2019. Geometrically nonlinear vibration analysis of sandwich nanoplates based on higher-order nonlocal strain gradient theory. *International Journal of Mechanical Sciences, 156***,** pp.31-45.

[28] Thai, C.H., Hung, P.T., Nguyen-Xuan, H. & Phung-Van, P., 2023. A size-dependent meshfree approach for magneto-electro-elastic functionally graded nanoplates based on nonlocal strain gradient theory. *Engineering Structures, 292***,** pp.116521.

[29] Kumar, D., Ali, S.F. & Arockiarajan, A., 2021. Theoretical and experimental studies on large deflection analysis of double corrugated cantilever structures. *International Journal of Solids and Structures, 228***,** pp.111126.

[30] Han, P., Tian, F. & Babaei, H., 2023. Thermally induced large deflection analysis of graphene platelet reinforced nanocomposite cylindrical panels. *Structures, 53,* pp.1046-1056.

[31] Bertóti, E., 2020. Primal- and dual-mixed finite element models for geometrically nonlinear shear-deformable beams – a comparative study. *Computer Assisted Methods in Engineering and Science, 27* (4), pp.285-315.

[32] Liu, L., Zhong, X. & Liao, S., 2023. Accurate solutions of a thin rectangular plate deflection under large uniform loading. *Applied Mathematical Modelling, 123,* pp.241-258.

[33] Wang, J. & Xiao, J., 2022. Analytical solutions of bending analysis and vibration of rectangular nano laminates with surface effects. *Applied Mathematical Modelling, 110,* pp.663-673.

[34] Mehar, K., Panda, S.K. & Mahapatra, T.R., 2018. Thermoelastic deflection responses of cnt reinforced sandwich shell structure using finite element method. *Scientia Iranica, 25* (5)**,** pp.2722-2737.

[35] Mehar, K., Panda, S.K. & Patle, B.K., 2018. Stress, deflection, and frequency analysis of cnt reinforced graded sandwich plate under uniform and linear thermal environment: A finite element approach. *Polymer Composites, 39* (10)**,** pp.3792-3809.

[36] Mehar, K. & Panda Subrata, K., 2017. Nonlinear static behavior of fg-cnt reinforced composite flat panel under thermomechanical load. *Journal of Aerospace Engineering, 30* (3)**,** pp.04016100.

[37] Mehar, K. & Panda, S.K., 2018. Elastic bending and stress analysis of carbon nanotube-reinforced composite plate: Experimental, numerical, and simulation. *Advances in Polymer Technology, 37* (6)**,** pp.1643-1657.

[38] Mehar, K., Panda, S.K. & Mahapatra, T.R., 2018. Large deformation bending responses of nanotube-reinforced polymer composite panel structure: Numerical and experimental analyses. *Proceedings of the Institution of Mechanical Engineers, Part G: Journal of Aerospace Engineering, 233* (5)**,** pp.1695-1704.

[39] Ambartsumian, S.A., 1960. On the theory of bending of anisotropic plates and shallow shells. *Journal of Applied Mathematics and Mechanics, 24* (2)**,** pp.500-514.

[40] Reddy, J.N., 1984. A simple higher-order theory for laminated composite plates. *Journal of Applied Mechanics, 51* (4)**,** pp.745-752.

[41] Reissner, E., 1975. On transverse bending of plates, including the effect of transverse shear deformation. *International Journal of Solids and Structures, 11* (5), pp.569-573.

[42] Touratier, M., 1991. An efficient standard plate theory. *International Journal of Engineering Science, 29* (8), pp.901-916.

[43] Soldatos, K.P., 1992. A transverse shear deformation theory for homogeneous monoclinic plates. *Acta Mechanica, 94* (3), pp.195-220.

[44] Aydogdu, M., 2009. A new shear deformation theory for laminated composite plates. *Composite Structures, 89* (1)**,** pp.94-101.

[45] Mantari, J.L., Oktem, A.S. & Guedes Soares, C., 2012. A new higher order shear deformation theory for sandwich and composite laminated plates. *Composites Part B: Engineering, 43* (3)**,** pp.1489-1499.

[46] Li, Q., Wu, D., Chen, X., Liu, L., Yu, Y. & Gao, W., 2018. Nonlinear vibration and dynamic buckling analyses of sandwich functionally graded porous plate with graphene platelet reinforcement resting on winkler–pasternak elastic foundation. *International Journal of Mechanical Sciences, 148***,** pp.596-610.

[47] Kerr, A.D. & Alexander, H., 1968. An application of the extended kantorovich method to the stress analysis of a clamped rectangular plate. *Acta Mechanica, 6* (2), pp.180-196.

[48] Bellman, R. & Casti, J., 1971. Differential quadrature and long-term integration. *Journal of Mathematical Analysis and Applications, 34* (2), pp.235-238.

[49] Mousavi, S.M. & Tahani, M., 2012. Analytical solution for bending of moderately thick radially functionally graded sector plates with general boundary conditions using multi-term extended kantorovich method. *Composites Part B: Engineering, 43* (3), pp.1405-1416.